# Brillouin light scattering investigation of the thickness dependence of Dzyaloshinskii-Moriya interaction in $Co_{0.5}Fe_{0.5}$ ultrathin films

M. Belmeguenai,[1,*] M. S. Gabor,[2,†] Y. Roussigné,[1] A. Stashkevich,[1,3] S. M. Chérif,[1] F. Zighem,[1] and C. Tiusan[2,4]

[1]*Laboratoire des sciences des procédés et des matériaux (LSPM), Centre national de la recherche scientifique (CNRS)-Université Paris 13, Sorbonne Paris Cité, 99 avenue Jean-Baptiste Clément Université Paris 13, 93430 Villetaneuse, France*

[2]*Center for Superconductivity, Spintronics and Surface Science, Technical University of Cluj-Napoca, Str. Memorandumului No. 28 RO-400114 Cluj-Napoca, Romania*

[3]*International Laboratory MultiferrLab, ITMO University, St. Petersburg 197101, Russia*

[4]*Institut Jean Lamour, CNRS, Université de Nancy, BP 70239, F-54506 Vandœuvre, France*

(Received 22 February 2016; revised manuscript received 15 April 2016; published 11 May 2016)

$Co_{0.5}Fe_{0.5}$ (CoFe) ultrathin films of various thicknesses ($0.8\,\text{nm} \leqslant t_{CoFe} \leqslant 1.6\,\text{nm}$) have been grown by sputtering on (001) MgO single crystal or $Si/SiO_2$ substrates, using Pt as capping or buffer layers, respectively. The x-ray diffraction revealed an in-plane epitaxial (isotropic) growth of Pt on MgO (Si). Their magnetic properties have been studied by vibrating sample magnetometry and Brillouin light scattering (BLS) in the Damon-Eshbach geometry. Vibrating sample magnetometry characterizations show that films grown on MgO are in-plane magnetized, while films deposited on Si are perpendicularly magnetized for CoFe thickness below 1.4 nm. The BLS measurements reveal a pronounced nonreciprocal spin waves propagation, which increases with decreasing CoFe thickness. This nonreciprocity was attributed to an interfacial Dzyaloshinskii-Moriya interaction (DMI) induced by Pt interface with CoFe. Moreover, the DMI sign has been found to depend on the stacks order: it is positive (negative) for CoFe/Pt (Pt/CoFe). The effective thickness dependence of the DMI effective constant shows two regimes due to the degradation of the interfaces as the CoFe thickness decreases. We thus show that the magnetic dead layer should be taken into account to precisely determine the surface DMI constant $D_s$. Therefore, for the thickest samples, the surface DMI constants are nearly opposite: $-1.27$ and $1.32\,\text{pJ m}^{-1}$ for Pt/CoFe and its reversed system, respectively.

DOI: 10.1103/PhysRevB.93.174407

## I. INTRODUCTION

Heavy metal/ferromagnet (HM/FM) heterostructures are drawing rapidly increasing interest in the scientific community due to their outstanding potential for technological innovations capable of revolutionizing the whole philosophy of magnetic memory and logic devices. However, no technological breakthrough is possible without major developments in fundamental science. Thus, the discovery of the spin Hall effect (SHE) [1–4] and its inverse [5–7], spin orbit torques [8], and most recently, the skyrmion (spin configurations at the nanoscale) [9–11] and domain wall (DW) chirality inversion in HM/FM bilayers resulted in a profound reassessment of the roles played by major physical mechanisms typically involved in nanomagnetism and spintronics. In particular, much higher velocities of current-driven DWs were reported in ultrathin ferromagnetic layers displaying large perpendicular magnetic anisotropy, which is only possible in the presence of spin-orbit torques in metals of large spin-orbit coupling, i.e. heavy metals. Although the initial suggestion was that these are the spin-currents induced through the SHE that are instrumental in the effect observed, now the opinion in the magnetic community is shifting towards the decisive role played in this phenomenon by the interfacial Dzyaloshinskii-Moriya interaction (DMI) [12,13].

The Dzyaloshinskii-Moriya effect is an antisymmetric exchange interaction that appears in ferromagnetic materials in the absence of spatial inversion symmetry, predicted by Dzyaloshinskii [12] as early as 1957 and revisited in more detail by Moriya three years later [13]. Nowadays, practically all the applications of thin magnetic films, however different, are unthinkable without nanostructuring unavoidably leading to breaking of symmetry. The latter applies directly to HM/FM bilayers, in which case DMI is localized in the immediate proximity of the interface and consequently is referred to as interfacial. It changes the static and dynamic properties of DWs [14]. It is also involved in creating and stabilizing chiral spin textures such as magnetic skyrmions [9–11], generally considered as promising candidates for the role of magnetic bits to carry and store information in the future. Importantly, it is also known to be responsible for the nonreciprocity of spin waves (SWs) propagation in asymmetric HM/FM bilayers [15,16]. The influence of DMI on wave behavior is realized through additional spin pinning of the circular components of the dynamic magnetization at the HM/FM interface. Since the Landau-Lifshitz equation is naturally formulated in the circular basis, the induced nonreciprocity simply scales with the DMI constant. In other words, there is no more direct and reliable means of quantifying the DMI strength than experimental estimation of the abovementioned nonreciprocity, typically by means of Brillouin light spectroscopy (BLS).

The DMI is usually characterized by its effective ($D_{\text{eff}}$) or surface ($D_s$) constants [17]. It is thus interesting for both application and fundamental research to determine precisely the sign and the value of the DMI constant. Several experimental [18–20] and theoretical studies [21,22], largely based on how this interaction alters the properties of DWs, were performed recently. However, the experimental evaluation of $D_{\text{eff}}$, using

*belmeguenai.mohamed@univ-paris13.fr
†mihai.gabor@phys.utcluj.ro

 

the abovementioned techniques, is at best indirect and based on strong assumptions about the dynamics of the DW. Moreover, any numerical estimation is to be checked experimentally. Therefore, a direct experimental measurement of $D_{\text{eff}}$ is required. Recently, it has been shown that the BLS can be effectively used for the direct measurement of $D_{\text{eff}}$ [17,23,24]. Indeed, when the static magnetization is in-plane and perpendicular to the SW wave vector (Damon-Eshbach geometry), the DMI interaction induces a characteristic nonreciprocity of the SW propagation. It is manifested by a difference between the frequencies of two SWs travelling in opposite directions and having the same wave number. The DMI constant determination is thus reduced to this simple frequency difference measurement. Therefore, in this paper, we use BLS combined with vibrating sample magnetometry (VSM) to measure the $Co_{0.5}Fe_{0.5}$ thickness dependence of DMI constants in Pt/$Co_{0.5}Fe_{0.5}$ and $Co_{0.5}Fe_{0.5}$/Pt ultrathin heterostructures. We show that both in-plane and perpendicularly magnetized $Co_{0.5}Fe_{0.5}$ films are subjected to DMI. Moreover, the effective constant is thickness and interface dependent; its sign depends on the stacks order.

## II. SAMPLES AND EXPERIMENTAL TECHNIQUES

Two sets of samples, consisting of Pt and $Co_{0.5}Fe_{0.5}$ (CoFe) stacks grown on Si and MgO substrates, have been used in this paper. For the first set, several layers of CoFe 1 nm $\leqslant t_{\text{CoFe}} \leqslant$ 1.6 nm were deposited at room temperature on a Si substrate covered with a 100 nm thick thermally oxidized $SiO_2$ layer by a magnetron sputtering system. Prior to the deposition of CoFe film, a Ta (3 nm)/Pt (3 nm) buffer bilayer was deposited on the substrate. Finally, CoFe layers were coated by a bilayer of MgO (1.8 nm)/Ta (2 nm). The second set consists of CoFe layers of variable thicknesses (0.8 nm $\leqslant t_{\text{CoFe}} \leqslant$ 1.6 nm) sputtered on MgO substrates using a 5 nm thick MgO buffer layer and a 4 nm thick Pt capping layer. In these heterostructures, the Pt layer induces DMI in the CoFe ultrathin layers; while the MgO layer is used for the purpose of inducing perpendicular anisotropy. The measurements presented here were performed at room temperature.

The crystal structure of the films was determined by x-ray diffraction (XRD) experiments using a four-circle diffractometer. Vibrating sample magnetometry has been used to measure the hysteresis loops of the samples, both with the field applied perpendicular and parallel to the sample plane, and to determine static magnetic parameters including the intrinsic value of the saturation magnetization $M_s$. In the BLS setup, the SWs, of a wave number ($k_{\text{sw}}$) in the range $0 - 20\,\mu\text{m}^{-1}$ ($k_{\text{sw}} = 4\pi \sin(\theta_{\text{inc}})/\lambda$, where $\theta_{\text{inc}}$ is the incidence angle), are probed (in backscattering configuration) by illuminating the sample with a laser having a wavelength $\lambda = 532$ nm. The magnetic field was applied perpendicular to the incidence plane, which allows for probing SWs propagating along the in-plane direction perpendicular to the applied field: Damon-Eshbach (DE) geometry where the DMI effect on the SWs nonreciprocity is maximal [24]. For each angle of incidence, the spectra were obtained after counting photons up to 19 h (especially for the highest incidence angles) to have well-defined spectra where the line position can be determined with accuracy better than 0.1 GHz. The Stokes (S, negative frequency shift relative to the incident light as a magnon was created) and anti-Stokes (AS, positive frequency shift relative to the incident light as a magnon was absorbed) frequencies, detected simultaneously, were then determined from Lorentzian fits to the BLS spectra. For identical interfaces, S and AS modes should have the same frequency. In the presence of DMI, the frequency difference between these two propagating SWs exists and increases with $k_{\text{sw}}$. Therefore, the DMI constants are determined from $k_{\text{sw}}$ dependence of the frequency difference between S and AS lines.

## III. RESULTS AND DISCUSSION

Figures 1(a) and 1(b) show x-ray $2\theta$-$\omega$ (out of plane) diffraction patterns for Ta (3 nm)/Pt (3 nm)/CoFe (1.6 nm)/MgO (1.8 nm) and MgO (5 nm)/CoFe (1.2 nm)/Pt (4 nm) structures grown on $Si/SiO_2$ and MgO (001) substrates, respectively. In the case of the films deposited on $Si/SiO_2$, the XRD pattern shows, besides the substrate reflection, only the presence of the Pt (111) reflection. However, a careful analysis of the XRD pattern indicates a slight asymmetry of the Pt diffraction peak and a relatively low intensity peak at lower angles, which could

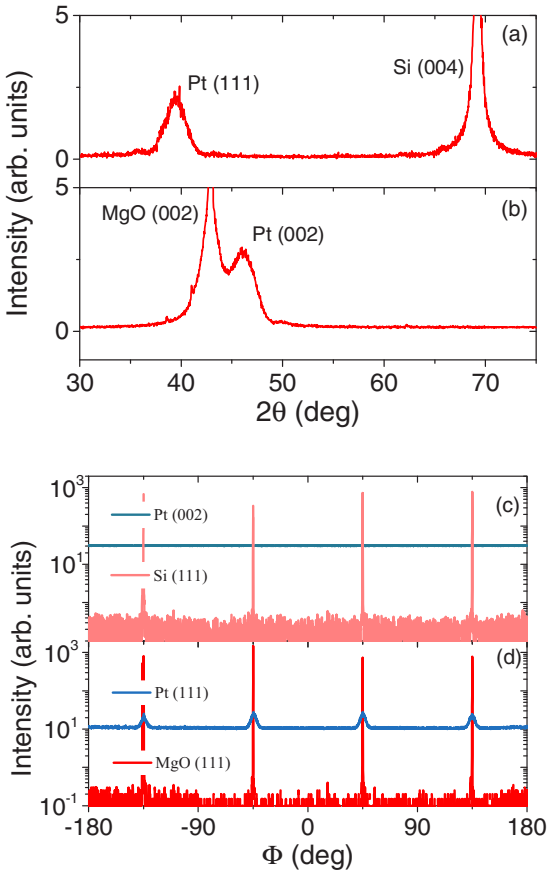


FIG. 1. X-ray $2\theta$-$\omega$ (out of plane) diffraction patterns for (a) $Si/SiO_2$//Ta (3 nm)/Pt (3 nm)/CoFe (1.6 nm)/MgO (1.8 nm)/Ta (2 nm) and (b) MgO//MgO (5 nm)/CoFe (1.2 nm)/Pt (4 nm) structures. Φ-scan measurements performed at a tilt angle $\Psi = 54.7^\circ$ probing (a) MgO and Pt (111) type reflections and (b) Pt (002) and Si (111) type reflections for samples grown on MgO and Si, respectively.

be attributed to the presence of the Ta buffer reflections. In the case of the structures grown on MgO, the XRD pattern shows only the Pt (002) and the substrate MgO (002) reflections. These results indicate a relatively strong out-of-plane (111) and (001) textured growth of the Pt films on $Si/SiO_2$ and MgO (001) substrates, respectively. In order to check a possible in-plane orientation of the Pt films, we have performed Φ-scan measurements, shown in Figs. 1(c) and 1(d). The Φ scans were carried out at a tilt angle $\Psi = 54.7^\circ$, and we have probed the (002) and (111) type reflections for Pt and the (111) type reflections for Si and MgO. In the case of the films grown on Si, no diffraction maxima were observed during the Φ scans, which suggest an in-plane isotropic distribution of the Pt crystallites. However, in the case of the films on MgO, distinct maxima corresponding to the Pt (111) type reflections are clearly seen. Moreover, the fact that these reflections are present at the same Φ angle as MgO (111) type reflections indicates that Pt grows with the following epitaxial relation: Pt(001)[100]//MgO(001)[100]. Due to the extremely low thickness of the CoFe films, we were unable to probe by XRD the orientation on the CoFe crystal. Nonetheless, the fact that, in the case of films on the Si substrate, the CoFe films are grown on Pt with isotropic in-plane crystalline distribution suggests that CoFe also has an isotropic in-plane crystallites distribution. To test this, we have performed angular remanent magnetization (ARM) measurements, by measuring the remanent magnetization ($M_r$) after saturation at different in-plane angles. Figure 2(a) shows the normalized ARM curve ($M_r/M_s$, where $M_s$ is the magnetization at saturation) for the Pt (3 nm)/CoFe (1.6 nm)/MgO (1.8 nm) structure grown on Si. The shape of the ARM curve is not perfectly isotropic but shows a slightly uniaxial character, as confirmed also by VSM hysteresis loops [Fig. 2(c)]. This uniaxial character is not unusual for sputtered films, and it is most likely due to a residual magnetic field present during growth, and it is not connected with the in-plane crystalline anisotropy. In contrast, for the films grown on MgO, the ARM curve [Fig. 2(b)] shows a clear fourfold symmetry with four distinct maxima and minima. This indicates the presence of an in-plane biaxial anisotropy with the easy axis at 45° with the substrate edges, as expected in the case of epitaxial growth. The fact that the ARM curve has a "butterfly" shape points out the presence of a small uniaxial anisotropy, most likely induced during growth, superimposed on the biaxial one [25]. This is confirmed also by the hysteresis loops in Fig. 2(d), which shows that the two hard axes are inequivalent due to the overlap of the uniaxial component.

In the case of the samples grown on Si, the VSM characterization revealed that thickest films ($t_{CoFe} > 1.2$ nm) are in-plane magnetized, while the thinner ones show a perpendicular magnetic anisotropy as shown in Fig. 2(e), where the typical perpendicular applied field hysteresis loop for 1.1 nm thick film is presented. The effective demagnetizing field ($H_a$) deduced from the linear part of the S-shaped hysteresis loops [Fig. 3(a)] increases with CoFe thickness, suggesting an interface contribution. Note that positive (negative) $H_a$ values refer to an in-plane (perpendicular to the plane) easy axis. In contrast, regardless of the thickness, the films deposited on MgO substrates are in-plane magnetized as indicated on Fig. 2(f), where the typical perpendicular applied field

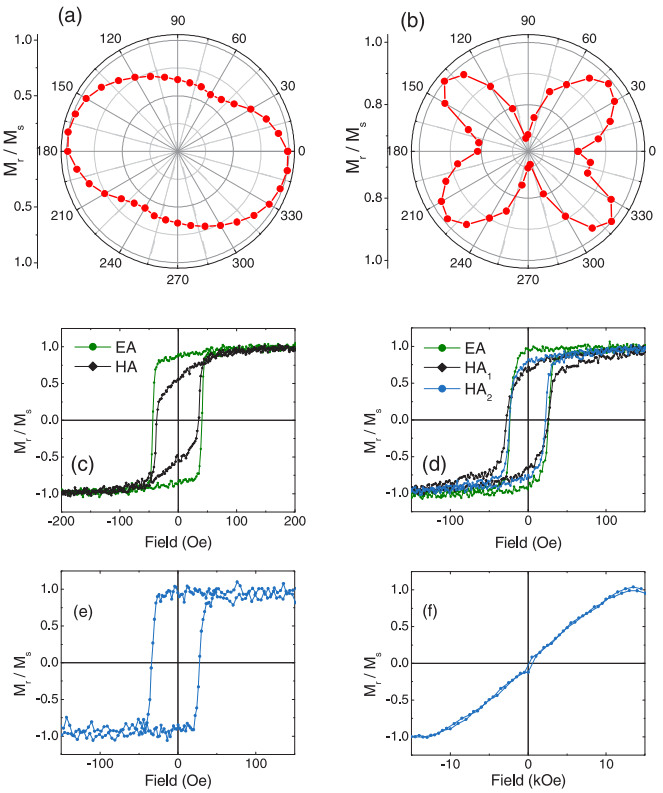


FIG. 2. (a) Angular remanent curve (ARM) for the Pt/CoFe (1.6 nm)/MgO sample showing a weak uniaxial character and (c) hysteresis loops measured along the easy (EA) and hard (HA) magnetization axis. (b) ARM curve for the MgO/CoFe (1.2 nm)/Pt sample indicating the presence of biaxial magnetic anisotropy superimposed by weak uniaxial component and (d) hysteresis loops along the easy (EA), hard ($HA_1$), and hardest ($HA_2$) magnetization axis. Out-of-plane hysteresis loops for (e) Pt/CoFe (1.1 nm)/MgO sample indicating the presence of perpendicular magnetic anisotropy and for (f) MgO/CoFe (1 nm)/Pt sample showing the presence of in-plane magnetic anisotropy.

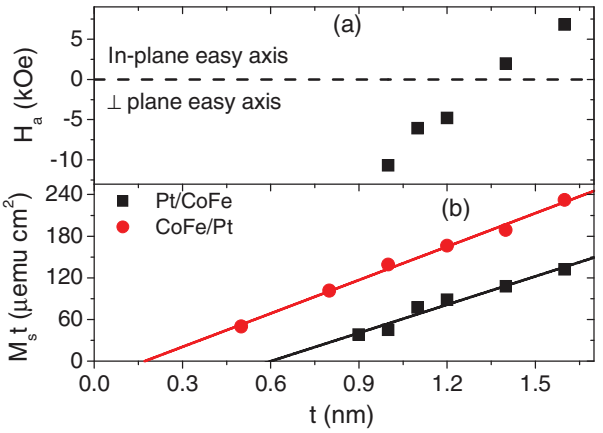


FIG. 3. Thickness dependences of (a) the effective perpendicular anisotropy field for CoFe thin films grown on Si substrates and (b) the saturation magnetic moment per unit area for CoFe thin films grown on both MgO and Si substrates. Symbols refer to measurements and solid lines are the linear fits. The effective perpendicular anisotropy fields have been obtained from the hard axis hysteresis loops.

hysteresis loop for 1 nm thick film is shown. This might be due to the different degree of oxidation of the CoFe layer deposited on MgO with respect to the CoFe layer on which MgO was deposited [26,27], but also to the different surfaces (111) and (001) of Pt in contact with CoFe [28] in the case of the films grown on Si or MgO, respectively.

Figure 3(b) shows the CoFe thickness dependences of the saturation magnetic moment per unit area for the films grown on Si and MgO substrates. These thickness dependences of the magnetic moment are used to determine the magnetization at saturation ($M_s$) and the magnetic dead layer thickness ($t_d$): the slope gives the saturation magnetization, while the horizontal axis intercept gives the extent of the dead layer, which might form due to intermixing and oxidation of the CoFe during MgO layer deposition. The thickness of the magnetic dead layer and magnetization at saturation are found to be 0.6 nm (0.17 nm) and $1356 \pm 70\,\mathrm{emu/cm^3}$ ($1602 \pm 70\,\mathrm{emu\,cm^{-3}}$) for the Pt/CoFe (CoFe/Pt) system. The larger magnetic dead layer for the Pt/CoFe system is most likely due to an enhanced oxidation of the CoFe layer when MgO is deposited on top [27]. Moreover, the increase of $M_s$ for the CoFe/Pt system is most probably connected to the lower magnetic dead layer thickness and to the improved crystalline quality of the CoFe films grown on MgO, as mentioned above. In the following, the BLS measurements were performed with the magnetization saturated in the film plane (along the substrate edge) under magnetic fields much higher than $-H_a$ (for spontaneously perpendicularly magnetized samples) deduced from the VSM hysteresis loops [Fig. 3(a)]. Figure 4(a) shows the typical BLS spectra for the 1.2 nm (perpendicular magnetized) and 1.4 nm (in-plane magnetized) thick samples grown on Si for $k_{sw} = 18.09\,\mu\mathrm{m}^{-1}$ ($\theta_{inc} = 50°$) and $4.10\,\mu\mathrm{m}^{-1}$ ($\theta_{inc} = 10°$). It reveals the existence of both S and AS spectral lines. Besides the usual intensity asymmetry of these lines due to the coupling mechanism between the light and SWs, a pronounced difference between the frequencies of the S and AS modes ($\Delta F = F_S - F_{AS}$), especially for higher values of $k_{sw}$, is revealed by the BLS spectra. This frequency mismatch is due to the interfacial DMI, as demonstrated previously [17,23,24]. Since the inverse proportionality on the ferromagnetic layer thickness is usually a signature of an interface effect, the behavior of $\Delta F$ versus $1/t_{CoFe}$ is presented in Fig. 4(b) for $k_{sw} = 20.45\,\mu\mathrm{m}^{-1}$ ($\theta_{inc} = 60°$) and $11.81\,\mu\mathrm{m}^{-1}$ ($\theta_{inc} = 30°$). It can be observed that $\Delta F$ increases with $1/t_{CoFe}$ and approaches zero when $t_{CoFe}$ tends to infinity, confirming the interfacial origin of the DMI. The variation of the S and AS frequency shifts versus $k_{sw}$ is shown in Fig. 4(c) for films grown on Si (for clarity, the data for the 1 nm thick film are not shown). The solid lines correspond to the fit for experimental data using Eq. (1) to describe the DE mode dispersion [15,23], taking into account the DMI contribution. For each sample, two branches, referring to S (black color) and AS (red color) lines, are presented. According to Eq. (1), the dispersion is split into two branches corresponding to the frequency shift in the Stokes $F_S$ and anti-Stokes $F_{AS}$ lines. Each one results from two contributions. While the major one, being field dependent, takes into account the dipole-dipole interactions linear in $k_{sw}$ (in ultrathin films as ours) and a quadratic in $k_{sw}$ contribution of the conventional isotropic exchange, the DMI contribution, linear in $k_{sw}$, is described by a smaller addition whose sign

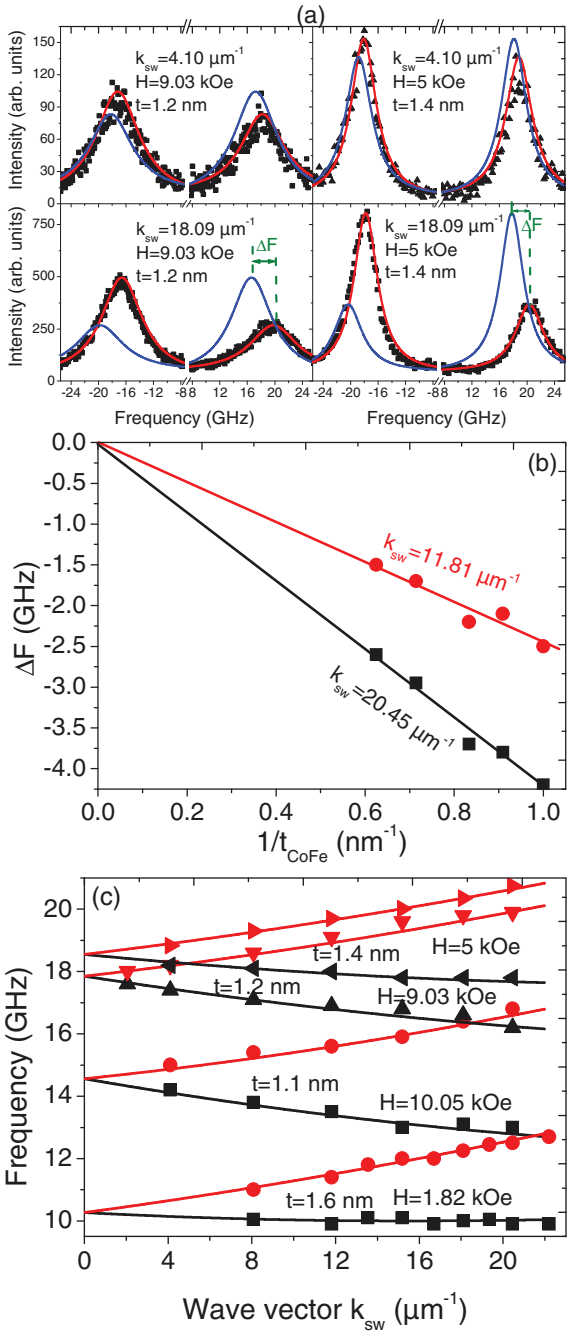


FIG. 4. (a) BLS spectra measured for Pt/CoFe (1.2 nm and 1.4 nm)/MgO films, grown on Si, at two different applied field values and at two characteristic light incidence angles corresponding to $k_{sw} = 18.09$ and $4.10\,\mu\mathrm{m}^{-1}$. Symbols refer to the experimental data, and solid lines are the Lorentzian fits. Fits corresponding to negative applied fields (blue lines) are presented for clarity and direct comparison of the S and AS frequencies. (b) Thickness dependence of the frequency difference $\Delta F$, of Pt/CoFe($t_{CoFe}$)/MgO films, grown on Si, for two characteristic light incidence angles corresponding to $k_{sw} = 20.45$ and $11.81\,\mu\mathrm{m}^{-1}$. Symbols refer to experimental data, and straight solid lines are used for eye guides. (c) Measured SW dispersion for Pt/CoFe($t_{CoFe}$)/MgO films, grown on Si. Symbols show the experimental BLS data for AS (red) and S frequencies (black). Solid lines represent the model described by Eq. (1) with effective DMI constants $D_{eff}$ presented in (b) and magnetic parameters given in the text.

depends on whether one is interested in the S or AS frequency shift. Importantly, if $F_S$ is lower than $F_{AS}$, then the resulting DMI constant is negative for positive applied magnetic field.

$$F = F_0 + F_{DMI} = \mu_0 \frac{\gamma}{2\pi} \sqrt{\left[H + Jk_{sw}^2 + P(k_{sw}t_{FM})M_s\right]\left[H + Jk_{sw}^2 - P(k_{sw}t_{FM})M_s\right] + M_{eff}} \pm \frac{\gamma}{\pi M_s} D_{eff} k_{sw}, \quad (1)$$

where $H$ is the in-plane applied field, $t_{FM}$ is the ferromagnetic layer thickness, $\gamma$ is the gyromagnetic coefficient [$\gamma/(2\pi) = 13.996g\,\mathrm{GHz\,T^{-1}}$, where $g$ is the Landé factor], $\mu_0$ is the permeability of vacuum, $J = \frac{2A_{ex}}{\mu_0 M_s}$ with $A_{ex}$ is the exchange stiffness constant, $H_k$ is the perpendicular uniaxial anisotropy field, $\mu_0 M_{eff} = \mu_0(M_s - H_k) = \mu_0 H_a = \mu_0 M_s - \frac{2K_\perp}{M_s}$ is the effective magnetization. The coefficient $P(k_{sw}t_{FM}) = 1 - \frac{1-\exp(-k_{sw}t_{FM})}{k_{sw}t_{FM}}$, describing dipolar interactions, reduces in thin films ($k_{sw}t_{FM} \ll 1$) to a simple $P(k_{sw}t_{FM}) = \frac{k_{sw}t_{FM}}{2}$, which makes this term linear in $k_{sw}t_{FM}$. It should be noticed that, in our case, $k_{sw}t_{FM} \approx 0.02$.

We define the interfacial DMI constant as $D_s = t_{FM} D_{eff}$. From this, the frequency difference can be inferred to be

$$\Delta F = F_S - F_{AS} = \frac{2\gamma}{\pi M_s} D_{eff} k_{sw} = \frac{2\gamma}{\pi M_s} \frac{D_s}{t_{FM}} k_{sw}. \quad (2)$$

Visually, the two dispersion branches in Fig. 4(c) demonstrate close linear behavior. Let us estimate the influence of each physical mechanism on it. Thus, the dipolar contribution, scaling with $P(k_{sw}t_{FM})$ and hence linear in $k_{sw}$, does not exceed 200 MHz, which makes them practically negligible. At the same time, the frequency variation due to the conventional exchange can be as high as 0.5 GHz. However, both abovementioned mechanisms do not influence the difference between the S and AS frequency asymmetry $\Delta F$. This is not the case of the asymmetric surface anisotropy, whose contribution to $\Delta F$ should not be overlooked [29]. In this regard, Eq. (1) does not take it into account and must be thus considered approximate. More sophisticated numerical analysis, using the surface anisotropy constant (evaluated below), estimates the error associated with this anisotropy as not exceeding 3 MHz, which is explained by ultralow thickness of the CoFe layer. In other words, it is absolutely negligible.

Figure 5(a) shows the $k_{sw}$ dependence of $\Delta F$ for CoFe thin films grown on both substrates, where a clear linear behavior can be observed. Note the negative (positive) sign of $\Delta F$ for films grown on Si (MgO) substrates, suggesting that the Pt buffer (capping) layer induces a negative (positive) DMI effective constant. This sign inversion with respect to the stack order confirms the interfacial origin of the DMI and is consistent with the three-site indirect exchange mechanism [30,31] proposed previously. In fact, Fert proposed in 1990 a mechanism of interaction between two spins of neighboring atoms $A_1$, $A_2$ of the FM at the interface with the HM layer [31]. The mechanism involves the nearest atom $B$ of HM [Figs. 5(b) and 5(c)]. The interaction energy reads $E = \boldsymbol{D}_{12}.(\boldsymbol{S}_1 \times \boldsymbol{S}_2)$ with $\boldsymbol{D}_{12} = D\boldsymbol{w}$, where $D$ is a scalar, $\boldsymbol{S}_1$ is the spin of $A_1$, $\boldsymbol{S}_2$ is the spin of $A_2$ and $\boldsymbol{w}$ is the unit vector along the direction $\boldsymbol{A}_1\boldsymbol{B} \times \boldsymbol{A}_2\boldsymbol{B}$. Therefore, the direction of $\boldsymbol{D}_{12}$ is determined by the cross product of $\boldsymbol{A}_1\boldsymbol{B}$ and $\boldsymbol{A}_2\boldsymbol{B}$. Thus, it depends on whether HM is used as a capping layer or as a buffer layer: $\boldsymbol{D}_{12}^{capping} = -\boldsymbol{D}_{12}^{buffer}$. Consequently, the observed DMI constants should be of opposite signs for CoFe/Pt and Pt/CoFe stacks, as we have experimentally observed.

In more detail, the change of sign can be explained through the propagating SWs as follows. The vector $\boldsymbol{w}$ can be defined by the relation $\boldsymbol{w} = \boldsymbol{u} \times \boldsymbol{n}$, where $\boldsymbol{u}$ is the unit vector from $A_1$ to $A_2$, and $\boldsymbol{n}$ is the interface normal from FM to HM. If $D$ is positive (negative) [Figs. 5(b) and 5(c)], then $E$ is minimal when $(\mathbf{S}_1 \times \mathbf{S}_2)$ lies along $-\boldsymbol{w}$ (along $\boldsymbol{w}$). It means that this energy favors a precession around $-\boldsymbol{w}$ (around $\boldsymbol{w}$).

Let us consider SWs in the ferromagnetic layer of the abovementioned stacks submitted to an in-plane saturating field $\boldsymbol{H}$. Let us assume that the SW propagates along the in-plane direction $\boldsymbol{u}$ perpendicular to the external field. If $D$ is positive (negative), then $E$ favors the magnetization precession around $\boldsymbol{n} \times \boldsymbol{u}$ (around $\boldsymbol{u} \times \boldsymbol{n}$). As this magnetization precession occurs around $\boldsymbol{H}$, the interaction with HM facilitates or hinders the precession depending on whether $\boldsymbol{H}$ and $\boldsymbol{n} \times \boldsymbol{u}$ are parallel or antiparallel. This is the reason why two SWs propagating in two opposite directions ($\boldsymbol{u}$ or $\boldsymbol{u}' = -\boldsymbol{u}$) present different frequencies when one interface involves HM: if the interaction with HM acts in the same way as the external field for a SW propagating in the direction $\boldsymbol{u}$, then its frequency is higher than that of the SW propagating in the opposite direction. The same argument applies for the stacking order effect ($\boldsymbol{n}$ or $\boldsymbol{n}' = -\boldsymbol{n}$): if the interaction with a HM top layer reinforces the effect of the external field, then the interaction with a bottom layer acts conversely. This behavior is illustrated in Figs. 5(b) and 5(c) for negative $D$.

The frequency difference mismatch between Pt/CoFe/MgO and its reversed structure [shown in Fig. 5(a)] might be caused by several factors: the quality of the interface with Pt (yielding different absolute value of $D_s$ induced by Pt capping and buffer layer), the saturation magnetization $M_s$ and effective FM thickness (different magnetic dead layer thickness), as explicitly indicated by Eq. (2). Moreover, since the DMI is an interface effect [32], its strength is also expected to be influenced by the different surfaces (111) and (001) with different packings of Pt in contact with the ferromagnetic material. Therefore, for systematic comparison between the two sets of samples, $D_s$ should be determined. From the slopes of the $k_{sw}$ dependences of $\Delta F$, the effective DMI constants have been extracted using Eq. (2) with $\gamma/(2\pi) = 30.35\,\mathrm{GHz\,T^{-1}}$, $A_{ex} = 25\,\mathrm{pJ\,m^{-1}}$, $M_s = 1356\,\mathrm{emu\,cm^{-3}}$ (for Pt buffered) and $M_s = 1602\,\mathrm{emu\,cm^{-3}}$ (for Pt capped samples) deduced from the fit of BLS data shown in Fig. 4(c) and the VSM measurements, respectively. The evolution of the obtained values of $D_{eff}$ as function of the inverse of the CoFe films nominal thickness are shown in Fig. 6(a) where a linear behavior can be observed, as predicted theoretically. Note the deviation from the linearity, in the case of Pt capped systems, as the CoFe thickness approaches 0.8 nm, most probably due to the interface degradation. The linear fit of the experimental values of $D_{eff}$ allows determination of a unique

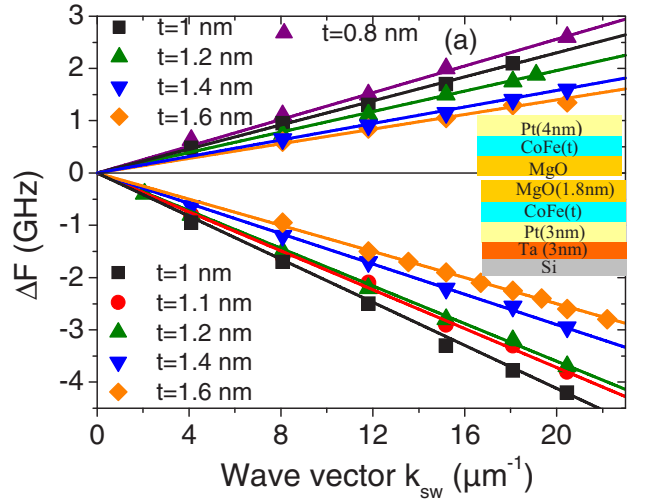


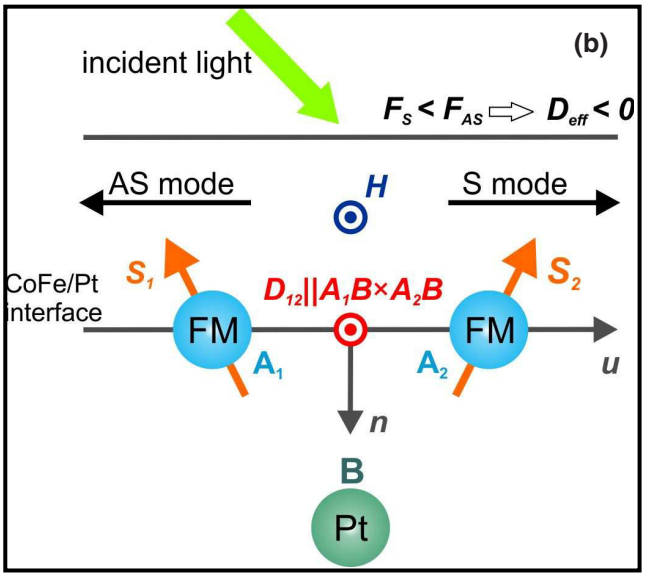


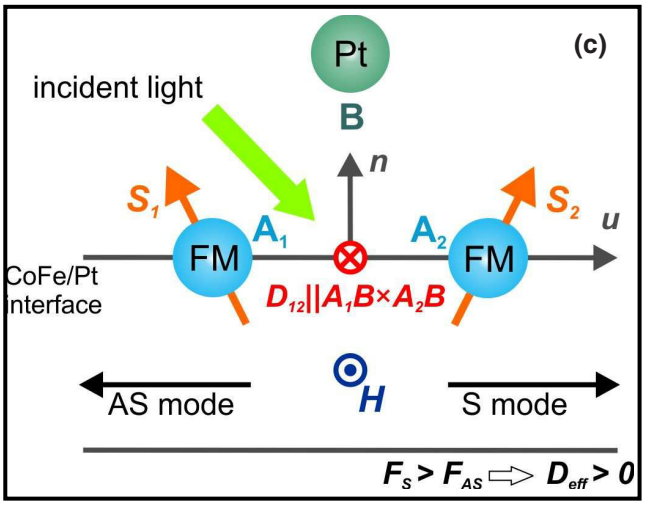


FIG. 5. (a) Wave vector ($k_{sw}$) dependence of the experimental frequency difference $\Delta F$ (symbols) Pt/CoFe($t_{CoFe}$)/MgO and MgO/CoFe($t_{CoFe}$)/Pt grown on Si and MgO substrates, respectively. Solid lines refer to linear fit using Eq. (2) and magnetic parameter in the text. Illustration of the stack order dependence of the DMI constant sign for negative $D$ in heterostructure composed of two ferromagnetic atoms $A_1$ and $A_2$ of spin $S_1$ and $S_2$ and HM atom $B$ (here Pt) used as (b) buffer or (c) capping layer. The direction of $\boldsymbol{D}_{12}$ is determined by the cross product of $\boldsymbol{A}_1\boldsymbol{B}$ and $\boldsymbol{A}_2\boldsymbol{B}$ ($\boldsymbol{D}_{12}//\boldsymbol{A}_1\boldsymbol{B}\times\boldsymbol{A}_2\boldsymbol{B}$), and therefore, the DMI constant sign depends on the stack order. Spin-waves (S and AS modes) propagating in two opposite directions ($\boldsymbol{u}$ or $\boldsymbol{u}'=-\boldsymbol{u}$) present different frequencies when one interface involves HM: (b) the interaction with HM reduces the effect of external field for a SW propagating in the direction $\boldsymbol{u}$ (S mode), and its frequency is lower than that of the SW propagating in the opposite direction (AS mode). (c) The interaction with HM acts in the same way as the external field for a SW propagating in the direction $\boldsymbol{u}$ (S mode), and its frequency is higher than that of the SW propagating in the opposite direction (AS mode).

value of the surface DMI constant: $D_s = -2.26\,\mathrm{pJ\,m^{-1}}$ and $D_s = 1.56\,\mathrm{pJ\,m^{-1}}$ for Pt/CoFe films and the reversed system, respectively. The $D_s$ value for Pt/CoFe films is higher than that of Pt/Co/$AlO_x$ ultrathin films [17]. This would make the studied structures especially attractive for DW chirality engineering [33]. The apparent difference between the absolute values of $D_s$ incites one to interpret the measured values of $D_{eff}$ in another way. To estimate precisely $D_s$ and the perpendicular anisotropy constant, the thickness of the dead layer should also be considered. First, let us consider the extracted effective magnetizations from the BLS measurements shown in Fig. 6(b) as a function of $1/(t_{CoFe}-t_d)$ for Pt/CoFe films. It can be seen that $M_{eff}$ follows a piecewise linear variation characterized by two regimes with a nominal critical CoFe thickness of 1.2 nm. Therefore, for each regime, the effective perpendicular anisotropy term $K_\perp$ could be phenomenologically separated in a volume and interfaces contributions and approximately obeys the relation $K_\perp = K_{v\perp} + \frac{K_{s\perp}}{t_{CoFe}-t_d}$. This allows us to derive the perpendicular surface anisotropy constants of $K_{\perp s} = 1.18\,\mathrm{mJ\,m^{-2}}$ and $K_{\perp s} = 0.62\,\mathrm{mJ\,m^{-2}}$ for thicker ($t_{CoFe} \geqslant 1.2$ nm: regime I) and thinner samples ($t_{CoFe} \leqslant 1.2$ nm: regime II), respectively. The extrapolation of $4\pi M_{eff}$ when $1/(t_{CoFe}-t_d)$ tends to zero allows one to derive the perpendicular volume anisotropy constants: $K_{\perp v} = -4.4\times 10^5\,\mathrm{J\,m^{-3}}$ and $K_{\perp v} = 4.6\times 10^5\,\mathrm{J\,m^{-3}}$ for thicker ($t_{CoFe} \geqslant 1.2$ nm) and thinner samples ($t_{CoFe} \leqslant 1.2$ nm), respectively. The surface (volume) anisotropies are in agreement with the ones deduced from the static measurements $K_s = 1.19\,\mathrm{mJ\,m^{-2}}$ ($K_{\perp v} = -4.8\times 10^5\,\mathrm{J\,m^{-3}}$) and $0.63\,\mathrm{mJ\,m^{-2}}$ ($K_{\perp v} = 3.2\times 10^5\,\mathrm{J\,m^{-3}}$) for thicker and thinner samples, respectively, shown on Fig. 6(c), where the effective surface energy $K_{eff}(t_{CoFe}-t_d) = K_{\perp s} + (K_{\perp v} - 2\pi M_s^2)(t_{CoFe}-t_d)$ is plotted versus the effective thickness $(t_{CoFe}-t_d)$. The static effective perpendicular magnetic anisotropy constant $K_{eff}$ was determined from $H_a$ [shown on Fig. 3(a)], using the relation $K_{eff} = -H_a M_s/2$. These two regimes may be related to a degradation of the interfaces for the thinner CoFe films, as it will be discussed below.

Let us now come back to the effective DMI constant. Interestingly, this thickness dependence deviates from the previous linear behavior when plotted versus the inverse of the corrected thickness of CoFe $[1/(t_{CoFe}-t_d)]$. Similar to the thickness dependence of the perpendicular anisotropy (Fig. 6), two regimes [above and below CoFe thickness of 1.2 nm (1 nm)

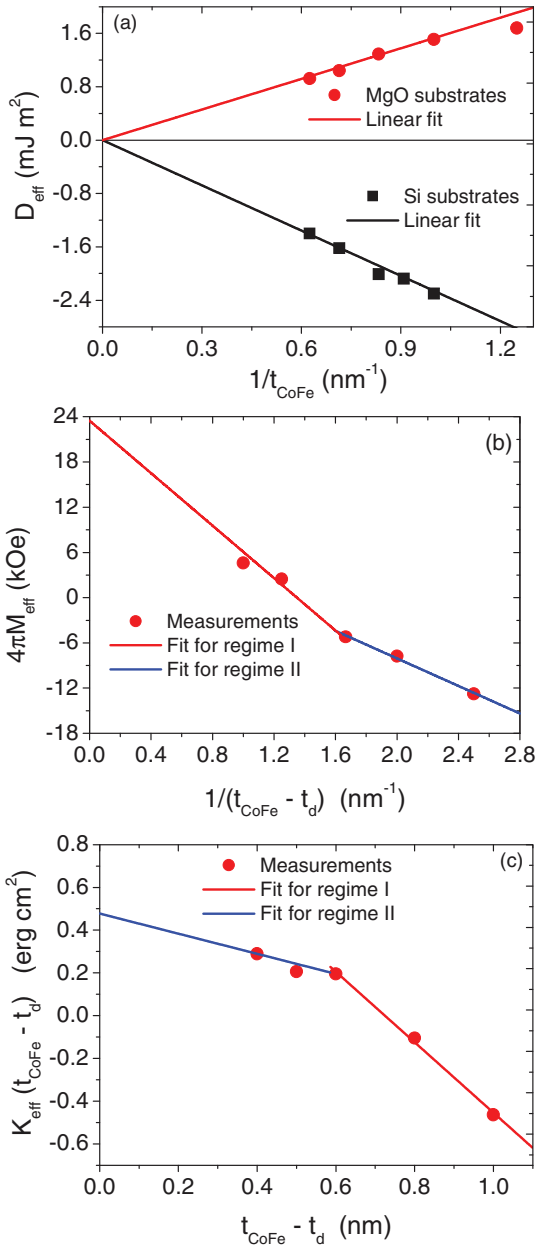


FIG. 6. Thickness dependence of (a) the effective DMI constants extracted from fits of Fig. 5(a). Solid lines refer to the linear fit for both systems (Pt/CoFe/MgO and its reversed structure). Thickness dependence of (b) the effective magnetization ($4\pi M_{\rm eff}$) extracted from the fit of BLS measurements and (c) the effective perpendicular surface anisotropy energy of Pt/CoFe($t_{\rm CoFe}$)/MgO grown on Si substrate. Solid red (blue) lines are the linear fits corresponding to $t_{\rm CoFe} \geqslant 1.2$ nm ($t_{\rm CoFe} \leqslant 1.2$ nm), respectively.

for Pt/CoFe (for CoFe/Pt)] with different slopes can be also distinguished as shown in Fig. 7: a slower dependence for $t_{\rm CoFe} \leqslant 1.2$ nm ($t_{\rm CoFe} \leqslant 1$ nm) is observed. Since both DMI and perpendicular anisotropy shown by our samples have an interfacial origin and since they present a similar thickness variation with the same critical thickness, the two regimes are most probably due to the degradation of the interface quality of the thin ferromagnetic layer, as shown above. Similar behavior has been observed for Pt/CoFeB/MgO systems [34]. By the

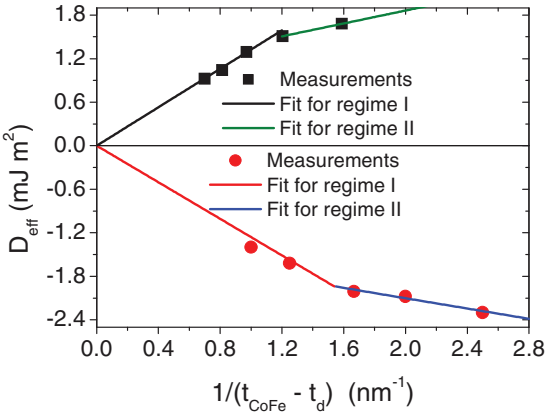


FIG. 7. Thickness dependence of the effective DMI constants of Pt/CoFe($t_{\rm CoFe}$)/MgO grown on Si substrate and MgO/CoFe($t_{\rm CoFe}$)/Pt grown on MgO substrate. Red (blue) and black (olive) fits correspond to $t_{\rm CoFe} \geqslant 1.2$ nm ($t_{\rm CoFe} \leqslant 1.2$ nm) and $t_{\rm CoFe} \geqslant 1$ nm ($t_{\rm CoFe} \leqslant 1$ nm) for Pt/CoFe and its reversed structure, respectively.

linear fit of the data of Fig. 7 for $t_{\rm CoFe} \geqslant 1.2$ nm (red lines) in the case of Pt/CoFe and for $t_{\rm CoFe} \geqslant 1$ nm (black lines) for the reversed structure, $D_s$ has been found to be $-1.27$ pJ m$^{-1}$ and 1.32 pJ m$^{-1}$ for Pt/CoFe and its reversed system, respectively. These values are slightly lower than that of Pt/Co/AlO$_x$ systems [17]. Taking into account the effective thickness, one obtains nearly opposite values of $D_s$ for Pt/CoFe and CoFe/Pt, as expected from the model of Fert [31]. Consequently, a vanishing of the frequency difference should occur for a symmetric structure HM/FM/HM. Moreover, it has to be mentioned that $D_s$ can be overestimated when the nominal and not the effective thickness is considered; an overestimation could be misguiding for applications.

It is worth mentioning that $\Delta F$ measurements (not shown here) for the magnetic applied field along the fourfold in-plane magnetization easy axis (45° with respect to the sample edges) of the films grown on MgO do not reveal a significant change in the DMI compared to the above case where it is applied along the fourfold hard axis.

The above obtained result allows classifying the investigated bilayers in terms of their applicability for skyrmion stabilization. According to recent theoretical predictions [35], there exist two threshold values distinguishing conventional bubbles from skyrmions, namely $D_{\rm eff} = 1.6$ mJ m$^{-2}$ for isolated skymion and $D_{\rm eff} = 2.1$ mJ m$^{-2}$ for skymion lattice ground state. This means that our Pt/CoFe samples, for example, fall into three major categories. First, the thickest sample with magnetic thickness $t_{\rm CoFe} - t_{\rm d} = 1$ nm (nominal thickness 1.6 nm) is not suitable for skyrmions. On the contrary, the thinnest with $t_{\rm CoFe} - t_{\rm d} = 0.4$ nm (nominal thickness 1.0 nm) is capable of stabilizing arrays of skyrmions. All the rest are good for individual skyrmions, but not for their arrays.

## IV. CONCLUSIONS

CoFe films of various thicknesses ($0.8\,{\rm nm} \leqslant t_{\rm CoFe} \leqslant 1.6\,{\rm nm}$) were prepared by sputtering on MgO and Ta/Pt-buffered Si/SiO$_2$ substrates. In the case of MgO, the CoFe

films have been capped with Pt. The VSM measurements revealed that, for MgO substrates, the CoFe films are in-plane magnetized over the investigated thickness range, while in-plane or perpendicular magnetized films, depending on the film thickness, were obtained for films grown on Si. Brillouin light scattering has been used in the Damon-Eshbach geometry to investigate the SWs nonreciprocity induced by the interfacial DMI. It turned out that the DMI effective constant sign depends on the stack order. The analysis of BLS measurements allowed deriving a surface DMI and perpendicular anisotropy constants. For the thickest samples (less sensitive to the dead layer effect), the surface DMI constants are nearly opposite: $-1.27\,\mathrm{pJ\,m^{-1}}$ and $1.32\,\mathrm{pJ\,m^{-1}}$ for Pt/CoFe and its reversed system, respectively. This makes these bilayers attractive for stabilization of individual and collective skyrmions.

## ACKNOWLEDGMENTS

This paper has been partially supported by the Conseil Régional, Île-de-France through the DIM C'Nano (IMADYN project) and the government of the Russian federation (Grant 074-U01). M.S.G. acknowledges the financial support of UEFISCDI through PN-II-RU-TE-2014-4-1820SPINCOD research Grant No. 255/01.10.2015. C.T. acknowledges the Exploratory Research Project, SPINTAIL PN-II-ID-PCE-2012-4-0315, No. 23/29.08.2013 for financial support.

[1] M. I. Dyakonov and V. I. Perel, Phys. Lett. A **35**, 459 (1971).
[2] J. E. Hirsch, Phys. Rev. Lett. **83**, 1834 (1999).
[3] S. Zhang, Phys. Rev. Lett. **85**, 393 (2000).
[4] S. O. Valenzuela and M. Tinkham, Nature **442**, 176 (2006).
[5] L. K. Werake, B. A. Ruzicka, and H. Zhao, Phys. Rev. Lett. **106**, 107205 (2011).
[6] E. Saitoh, M. Ueda, H. Miyajima, and G. Tatara, Appl. Phys. Lett. **88**, 182509 (2006).
[7] M. V. Costache, M. Sladkov, S. M. Watts, C. H. van der Wal, and B. J.van Wees, Phys. Rev. Lett **97**, 216603 (2006).
[8] S. Woo, M. Mann, A. J. Tan, L. Caretta, and G. S. D. Beach, Appl. Phys. Lett. **105**, 212404 (2014).
[9] X. Z. Yu, Y. Onose, N. Kanazawa, J. H. Park, J. H. Han, Y. Matsui, N. Nagaosa, and Y. Tokura, Nature **465**, 901 (2010).
[10] S. Heinze, K. von Bergmann, M. Menzel, J. Brede, A. Kubetzka, R. Wiesendanger, G. Bihlmayer, and S.Blügel. Nature Phys. **7**, 713 (2011).
[11] S. X. Huang and C. L. Chien, Phys. Rev. Lett. **108**, 267201 (2012).
[12] I. E. Dzialoshinskii, Sov. Phys. JETP **5**, 1259 (1957).
[13] T. Moriya, Phys. Rev. **120**, 91 (1960).
[14] A. Thiaville, S. Rohart, E. Jué, V. Cros, and A. Fert, Europhy. Lett. **100**, 57002 (2012).
[15] M. Kostylev, J. Appl. Phys. **115**, 233902 (2014).
[16] J. H. Moon, S. M. Seo, K. J. Lee, K. W. Kim, J. Ryu, H. W. Lee, R. D. McMichael, and M. D. Stiles, Phys. Rev. B **88**, 184404 (2013).
[17] M. Belmeguenai, J-P. Adam, Y. Roussigné, S. Eimer, T. Devolder, J-V. Kim, S. M. Chérif, A. Stashkevich, and A. Thiaville, Phys. Rev. B **91**, 180405(R) (2015).
[18] J. Torrejon, J. Kim, J. Sinha, S. Mitani, M. Hayashi, M. Yamanouchi, and H. Ohno, Nat. Commun. **5**, 4655 (2014).
[19] S. Pizzini, J. Vogel, S. Rohart, L. D. Buda-Prejbeanu, E. Jué, O. Boulle, I. M. Miron, C. K. Safeer, S. Auffret, G. Gaudin, and A. Thiaville, Phys. Rev. Lett. **113**, 047203 (2014).
[20] S. Emori, E. Martinez, K.-J. Lee, H.-W. Lee, U. Bauer, S.-M. Ahn, P. Agrawal, D. C. Bono, and G. S. D. Beach, Phys. Rev. B **90**, 184427 (2014).
[21] F. Freimuth, S. Blügel, and Y. Mokrousov, J. Phys. Condens. Matter **26**, 104202 (2014).
[22] B. Zimmermann, M. Heide, G. Bihlmayer, and S. Blügel, Phys. Rev. B **90**, 115427 (2014).
[23] K. Di, V. L. Zhang, H. S. Lim, S. C. Ng, M. H. Kuok, J. Yu, J. Yoon, X. Qiu, and H. Yang, Phys. Rev. Lett. **114**, 047201 (2015).
[24] V. L. Zhang, K. Di, H. S. Lim, S. C. Ng, M. H. Kuok, J. Yu, J. Yoon, X. Qiu, and H. Yang, Appl. Phys. Lett. **107**, 022402 (2015).
[25] M. S. Gabor, T. Petrisor Jr., C. Tiusan, M. Hehn, and T. Petrisor, Phys. Rev. B **84**, 134413 (2011).
[26] W. X. Wang, Y. Yang, H. Naganuma, Y. Ando, R. C. Yu, and X. F. Han, Appl. Phys. Lett. **99**, 012502 (2011).
[27] J. C. Read, P. G. Mather, and R. A. Buhrman, Appl. Phys. Lett. **90**, 132503 (2007).
[28] S. Kim, S. Lee, J. Kim, J. Kang, and J. Hong, J. Appl. Phys. **109**, 07B766 (2011).
[29] A. A. Stashkevich, M. Belmeguenai, Y. Roussigné, S. M. Cherif, M. Kostylev, M. Gabor, D. Lacour, C. Tiusan, and M. Hehn, Phys. Rev. B **91**, 214409 (2015).
[30] A. Fert, V. Cros, and J. Sampaio, Nat. Nanotechnol. **8**, 152 (2013).
[31] A. Fert, Mat. Sc. Forum **59-60**, 439 (1990).
[32] H. Yang, A. Thiaville, S. Rohart, A. Fert, and M. Chshiev, Phys. Rev. Lett. **115**, 267210 (2015).
[33] S. Emori, U. Bauer, S-M. Ahn, E. Martinez, and G. S. D. Beach, Nature Mater. **12**, 611 (2013).
[34] J. Cho, N.-H. Kim, S. Lee, J.-S. Kim, R. Lavrijsen, A. Solignac, Y. Yin, D.-S. Han, N. J. J. van Hoof, H. J. M. Swagten, B. Koopmans, and C.-Y. You, Nat. Commun. **6**, 7635 (2015).
[35] C. Moreau-Luchaire, C. Moutafis, N. Reyren, J. Sampaio, C. A. F. Vaz, N. Van Horne, K. Bouzehouane, K. Garcia, C. Deranlot, P. Warnicke, P. Wohlhüter, J.-M. George, M. Weigand, J. Raabe, V. Cros, and A. Fert, Nature Nanotechnology **11**, 444 (2016).